

Capillary Pressure Correlation for Mixed-Wet Reservoirs

S.M. Skjæveland, SPE, L.M. Siqueland, and A. Kjosavik, SPE, Stavanger College; W.L. Hammervold Thomas, SPE, Statoil; and G.A. Virnovsky, SPE, RF-Rogaland Research

Summary

For water-wet reservoirs, several expressions may be used to correlate capillary pressure, or height above the free water level, with the water saturation. These correlations all feature a vertical asymptote at the residual water saturation where the capillary pressure goes to plus infinity.

We have developed a general capillary pressure correlation that covers primary drainage, imbibition, secondary drainage, and hysteresis scanning loops. The graph exhibits an asymptote at the residual saturation of water and of oil where the capillary pressure goes to plus and minus infinity, respectively. The shape of the correlation is simple yet flexible as a sum of two terms, each with two adjustable parameters and is verified by laboratory experiments and well-log data. An associated hysteresis scheme is also verified by experimental data.

The correlation can be used to make representative capillary pressure curves for numerical simulation of reservoirs with varying wettability and to model and interpret flooding processes.

Introduction

Many capillary pressure correlations have been suggested in the literature,¹⁻⁵ and they typically have two adjustable parameters. One parameter expresses the pore size distribution and hence the curvature of the p_c curve, the other the actual level of the capillary pressure, i.e., the entry or the mean capillary pressure.

Most of the correlations are limited to primary drainage and positive capillary pressures. Huang *et al.*⁵ extended their correlation to include all four branches of the bounding hysteresis loop: spontaneous and forced imbibition, and spontaneous and forced secondary drainage. They employed the same primary drainage expression to each branch, scaled to fit the measured $p_c=0$ axis crossing.

We have chosen to base the general capillary pressure correlation for mixed-wet reservoir rock on the simple power-law form of Brooks and Corey^{2,3} for primary drainage capillary pressure from $S_w=1$ to S_{wR} . The classical expression for a water-wet core may be slightly rewritten to facilitate the extension of scope,

$$p_{cd} = \frac{c_{wd}}{\left(\frac{S_w - S_{wR}}{1 - S_{wR}}\right)^{a_{wd}}}, \quad (1)$$

where c_{wd} is the entry pressure, $1/a_{wd}$ the pore size distribution index,⁶ and S_{wR} the residual (irreducible) water saturation. The main reason for choosing this basis is the experimental verification of Eq. 1^{2,3} and its simplicity.

According to Morrow,⁷ there is now wide acceptance of the view that most reservoirs are at wettability conditions other than completely water-wet. To our knowledge, however, no comprehensive, validated correlation has been published for mixed-wet reservoirs. The lack of correlation makes it difficult to properly model displacement processes where imbibition is of importance and data are scarce, e.g., bottom water drive and water-alternate-gas injection.

In this article, we present a general capillary pressure correlation and an associated hysteresis loop scheme. We try to demonstrate the applicability of the correlation by fitting data from a series of membrane and centrifuge experiments on fresh cores, and we show that the correlation is well suited to represent measured capillary pressure curves over a wide range of rock types. Also, by analyzing well-log data from the same well in a bottom-water driven North Sea sandstone reservoir at several points in time, we are able to model the transition from the initial primary drainage saturation distribution to the later observed imbibition profile.

The correlation crosses the zero capillary pressure axis at two points for the imbibition and the secondary drainage branches. These points, together with the residual saturations, define the Amott-Harvey wettability index.⁷ Thus, variations in wettability, e.g., with height, could be incorporated into the correlation.

We adopt the terminology of Morrow⁷ to characterize the capillary pressure curve, **Fig. 1**: “drainage” denotes a fluid flow process where the water saturation is decreasing, even for an oil-wet porous medium; “imbibition” denotes a process where the oil saturation is decreasing; “spontaneous” imbibition occurs for positive capillary pressure, “forced” imbibition for negative capillary pressure; “spontaneous” (secondary) drainage occurs for negative capillary pressure, and “forced” (secondary) drainage for positive capillary pressure; “primary” drainage denotes the initial drainage process starting from $S_w=1.0$; and, for completeness, “primary” imbibition denotes a imbibition process starting from $S_o=1$.

Correlation

The design idea for the correlation is as follows: Eq. 1 is valid for a completely water-wet system and, if index w for water is substituted by index o , it is equally valid for a completely oil-wet system. For other cases between these limits, a correlation should be symmetrical with respect to the two fluids since neither dominates the wettability. One way to achieve a symmetrical form that is correct in the extremes is to sum the two limiting expressions, i.e., to sum the water branch given by Eq. 1 and a similar oil branch, resulting in the general expression,

$$p_c = \frac{c_w}{\left(\frac{S_w - S_{wR}}{1 - S_{wR}}\right)^{a_w}} + \frac{c_o}{\left(\frac{S_o - S_{oR}}{1 - S_{oR}}\right)^{a_o}}. \quad (2)$$

The a 's and c 's are constants and there is one set for imbibition and another for drainage. An imbibition curve from S_{wR} to S_{oR} is modeled by Eq. 2 and the four constants (a_{wi} , a_{oi} , c_{wi} , c_{oi}), and a secondary drainage curve from S_{oR} to S_{wR} by the constants (a_{wd} , a_{od} , c_{wd} , c_{od}).

The constraints on the constants are that a_w , a_o , c_w are positive numbers and c_o is a negative number. The plot of Eq. 2, both for imbibition and drainage, therefore consists of two branches, a positive water branch with an asymptote at $S_w=S_{wR}$ and a negative oil branch with an asymptote at $S_o=S_{oR}$, **Fig. 1**. Depicted in **Fig. 1** are (1) the primary drainage curve starting at $S_w=1$, modeled by Eq. 2 with $c_o=0$ and c_w equal to the entry pressure; (2) the primary imbibition curve from Eq. 2 with $c_w=0$ and c_o equal to the entry pressure of water into a 100% oil saturated core; and (3) the bounding (secondary) imbibition and secondary drainage curves forming the largest possible hysteresis loop.

It should be noted that we have not performed any systematic study to check if the primary drainage constants c_{wd} and a_{wd} in

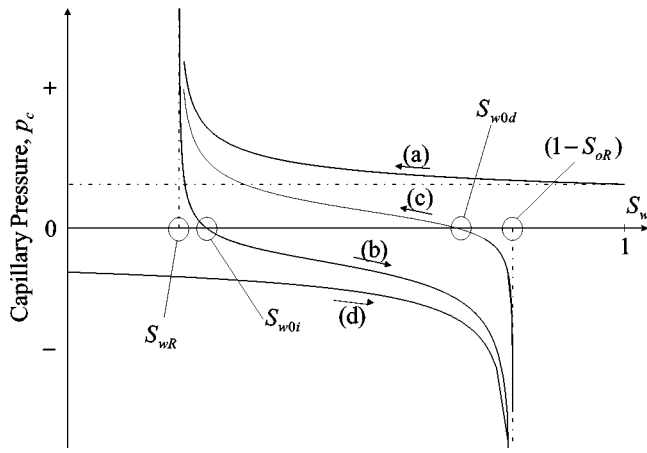


Fig. 1—Schematic of bounding curves, capillary pressure p_c as a function of water saturation S_w : (a) primary drainage; (b) (secondary) imbibition; (c) secondary drainage; (d) primary imbibition.

Eq. 1 may have the same values as those in the secondary drainage curve, Eq. 2 with the constants $(a_{wd}, a_{od}, c_{wd}, c_{od})$, or if two different sets of (a_{wd}, c_{wd}) are necessary. For simplicity, unless challenged by data to the contrary, we will assume that a single set suffices.

For imbibition, the graph crosses the zero capillary pressure axis at S_{w0i} , i.e., $p_c(S_{w0i})=0$, giving the following expressions for c_{oi} from Eq. 2:

$$c_{oi} = - \frac{c_{wi} \left(\frac{1 - S_{w0i} - S_{oR}}{1 - S_{oR}} \right)^{a_{oi}}}{\left(\frac{S_{w0i} - S_{wR}}{1 - S_{wR}} \right)^{a_{wi}}}, \quad (3a)$$

and for secondary drainage, $p_c(S_{w0d})=0$, gives

$$c_{od} = - \frac{c_{wd} \left(\frac{1 - S_{w0d} - S_{oR}}{1 - S_{oR}} \right)^{a_{od}}}{\left(\frac{S_{w0d} - S_{wR}}{1 - S_{wR}} \right)^{a_{wd}}}. \quad (3b)$$

The wettability index to water, I_{ww} , is given by⁷ $I_{ww} = (S_{w0i} - S_{wR}) / (1 - S_{oR} - S_{wR})$, and to oil, $I_{wo} = (1 - S_{w0d} - S_{oR}) / (1 - S_{oR} - S_{wR})$, and the Amott-Harvey wettability index⁷ is $I_{wAH} = I_{ww} - I_{wo}$. For a completely water-wet system, $I_{ww} = 1$ and $I_{wo} = 0$ giving $S_{w0i} = S_{w0d} = (1 - S_{oR})$, and from Eqs. 3, $c_{oi} = 0$ and $c_{od} = 0$. That is, Eq. 2 is used with only the water branch for both imbibition and drainage.

Wettability may vary with depth and be correlated with S_{wR} , as discussed by Jerauld and Rathmell.⁸ Incorporating such variations into the capillary pressure correlation would require additional functional relationships between the parameters in Eqs. 3, e.g., if the reservoir becomes more water-wet as the water-oil contact is approached from above, both zero point crossings, S_{w0i} and S_{w0d} , should approach $(1 - S_{oR})$, and c_{oi} and c_{od} go to zero. Also, if the interfacial tension is reduced for some displacement process, the c 's should go to zero proportionally, and S_{oR} and S_{wR} should approach zero.

One could consider putting Eq. 2 into dimensionless form by an extended J function,⁹ but it is not clear if this approach is valid for an imbibition process, as discussed earlier by Hamon and Pellerin.¹⁰ From their Fig. 8, it seems that the water branch of Eq. 2 could be scaled by the J function, but that the oil branch is almost independent of permeability and would require a different scaling group.

Hysteresis Loop Logic

Introduction. The hysteresis loop logic of Killough¹¹ is often employed in reservoir simulators. Its limitations have recently been discussed by Tan,¹² by Kriebner and Heinemann,¹³ and by Kleppe *et al.*¹⁴ who point out that Killough's method often is inadequate since it was formulated for the case where the drainage and imbibition curves meet at the residual oil saturation. To remedy this, it is suggested,^{13,14} with some modifications,¹⁴ to apply Land's¹⁵ expression,

$$\frac{1}{S_{oR}[1]} - \frac{1}{S_o[1]} = C, \quad (4)$$

where $S_o[1]$ is the start saturation of an imbibition process, on the primary drainage curve, and $S_{oR}[1]$ is the end saturation of the imbibition process, and C is Land's trapping constant.

A further limitation of Killough's procedure is that, on the third reversal, an artificial jump back to the first reversal curve is made to ensure that the reversal scanning curves proceed back to the point where the original bounding curve was left, an experimental fact.

Design Constraints. We consider the following design constraints for capillary pressure hysteresis loops to be generally accepted based on experimental evidence.¹⁶⁻²⁰

1. A first saturation reversal from the primary drainage curve, before reaching the residual water saturation S_{wR} , starts an imbibition scanning curve down to a residual oil saturation which is a certain fraction of S_{oR} , as determined by Eq. 4.

2. If the reversal from the primary drainage curve occurs at S_{wR} , the scanning curve scans to S_{oR} and is denoted the bounding imbibition curve.

3. A second reversal from S_{oR} defines a (secondary) drainage bounding curve that scans back to S_{wR} . Together, the bounding imbibition and drainage curves constitute the closed bounding hysteresis loop.

4. All scanning curves originating on the bounding imbibition curve scan back to S_{wR} , and all reversals on the bounding drainage curve spawn scans back to S_{oR} .

5. A scanning curve originating at $S_w[k]$, the water saturation at the start of the k th reversal curve, will scan back to $S_w[k-1]$ and form a closed scanning (hysteresis) loop, unless a new reversal occurs.

6. If a curve scanning back from $S_w[k]$ reaches $S_w[k-1]$ before any new reversal, i.e., it forms a closed scanning loop, the process continues by retracing the scan of the $k-2$ reversal as if the $k-1$ reversal had not occurred.

7. The shapes of the scanning loops are similar to the shape of the bounding loop.

Procedure. Let $S_w[k]$ denote the water saturation at the k th reversal and let $[k]$ also label properties of the scanning curve after the k th reversal with the convention that odd numbers denote imbibition and even numbers drainage. We will use the asymptotes $S_{wR}[k]$ and $S_{oR}[k]$ as scanning loop residual saturations and S_{wR} and S_{oR} as the bounding loop residual saturations.

First Reversal. The historic two-phase flooding process of a reservoir rock sample is usually primary drainage from $S_w = 1$. The first reversal will then be an imbibition curve denoted by $p_{ci}[1]$ originating from the primary drainage curve, $p_{cd}[0]$, Eq. 1. The reversal saturation $S_w[1]$ is a point on both the $p_{cd}[0]$ and the $p_{ci}[1]$ graph, that is,

$$p_{cd}[0](S_w[1]) = p_{ci}[1](S_w[1]), \quad (5a)$$

and where explicitly, from Eqs. 1 and 2,

$$p_{cd}[0](S_w[1]) = \frac{c_{wd}}{\left(\frac{S_w[1] - S_{wR}}{1 - S_{wR}} \right)^{a_{wd}}}, \quad (5b)$$

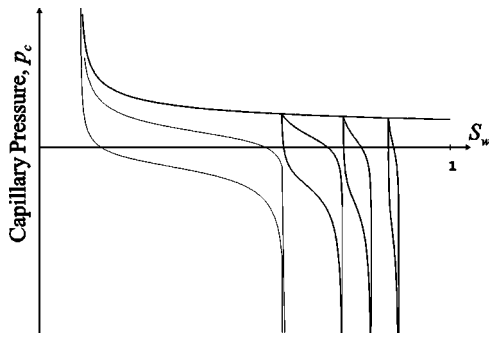


Fig. 2—Scanning loops with first reversal on the primary drainage curve and second reversal at the respective residual oil saturation.

$$p_{ci}[1](S_w[1]) = \frac{c_{wi}}{\left(\frac{S_w[1] - S_{wR}[1]}{1 - S_{wR}[1]}\right)^{a_{wi}}} + \frac{c_{oi}}{\left(\frac{S_o[1] - S_{oR}[1]}{1 - S_{oR}[1]}\right)^{a_{oi}}} \quad (5c)$$

To honor Eq. 5(a), we have to choose one parameter to be adjusted. Considering the design constraints, we keep all a 's and c 's constant for a given rock fluid and adjust the water branch asymptote of the scanning curve, i.e., $S_{wR}[1]$. The oil branch asymptote, $S_{oR}[1]$, is determined by Land's expression, Eq. 4. With this choice, the scanning curve will have a similar shape as the bounding imbibition curve since $(a_{wi}, a_{oi}, c_{wi}, c_{oi})$ are the same. The scanning curve may be considered to be part of a compression of the bounding imbibition curve between the two new asymptotes $S_{wR}[1]$ and $S_{oR}[1]$.

In summary, the first reversal imbibition curve $p_{ci}[1](S_w)$ starts on the primary drainage curve at the reversal point $S_w[1]$ and scans downward towards the asymptote $S_{oR}[1]$, as shown in Fig. 2 for three values of $S_w[1]$. Also shown in Fig. 2 is the bounding imbibition curve from S_{wR} , which is the minimum value of $S_w[1]$, back to S_{oR} . All curves in Fig. 2 are produced with a constant set of parameters. Only the residual saturations (asymptotes) are varied. These manufactured curves nicely reproduce the features of the many experimental curves presented by Wardlaw and Taylor.¹⁷

Second Reversal From Residual Oil Saturation. The three (secondary) drainage scanning curves from the three $S_{oR}[1]$ values and the bounding drainage curve from S_{oR} are also shown in Fig. 2, and they form four closed loops with their respective imbibition curves. The drainage scanning curves are generated by setting

$$p_{cd}[2](S_w[1]) = p_{cd}[0](S_w[1]), \quad (6a)$$

that is, the drainage curve following the second reversal, $p_{cd}[2]$, has to scan back to the first reversal point to make a closed loop. Here,

$$p_{cd}[2](S_w[1]) = \frac{c_{wd}}{\left(\frac{S_w[1] - S_{wR}[2]}{1 - S_{wR}[2]}\right)^{a_{wd}}} + \frac{c_{od}}{\left(\frac{S_o[1] - S_{oR}[2]}{1 - S_{oR}[2]}\right)^{a_{od}}}, \quad (6b)$$

and $S_{oR}[2] = S_{oR}[1]$. The only unknown in Eq. 6a is then $S_{wR}[2]$, which can be calculated, and the scanning curve is defined.

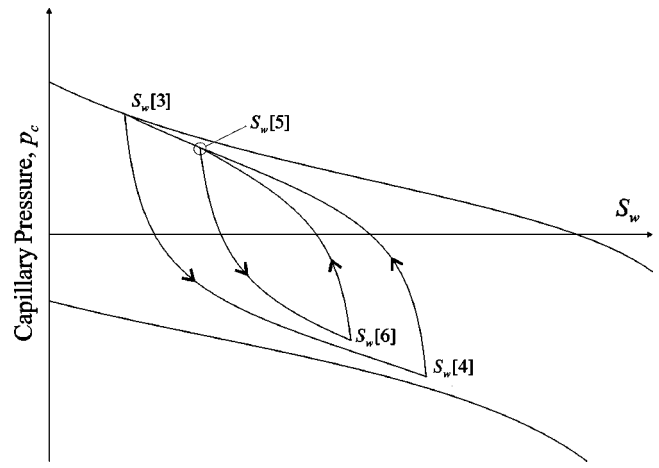


Fig. 3—Family of scanning loops spawned from a reversal point on the secondary drainage bounding curve.

Second General Reversal. If a second reversal should occur at a point $S_w[2]$ on the $p_{ci}[1](S_w)$ curve, before reaching $S_{oR}[1]$, a reversal drainage scanning curve, $p_{cd}[2](S_w)$, is spawned,

$$p_{cd}[2](S_w) = \frac{c_{wd}}{\left(\frac{S_w - S_{wR}[2]}{1 - S_{wR}[2]}\right)^{a_{wd}}} + \frac{c_{od}}{\left(\frac{S_o - S_{oR}[2]}{1 - S_{oR}[2]}\right)^{a_{od}}}, \quad (7)$$

scanning back to $S_w[1]$. The imbibition scanning curve $p_{ci}[1]$ from $S_w[1]$ and the drainage scanning curve $p_{cd}[2]$ back again from $S_w[2]$ have to be equal at the two reversal points to form a closed loop, i.e.,

$$p_{ci}[1](S_w[1]) = p_{cd}[2](S_w[1]) \quad (8a)$$

and

$$p_{ci}[1](S_w[2]) = p_{cd}[2](S_w[2]). \quad (8b)$$

These two equations determine the two new asymptotes $S_{wR}[2]$ and $S_{oR}[2]$ of $p_{cd}[2]$ in Eq. 7. As for the previous cases, we consider the a 's and the c 's to be invariant and adjust the vertical asymptotes of the scanning curve to get a closed loop. Thus the second scanning curve will be part of a compression of the secondary drainage curve between the two asymptotes $S_{wR}[2]$ and $S_{oR}[2]$.

Numerically, Eqs. 8 can be solved as follows: Let the first estimate of $S_{wR}[2]$ be the previous value, $S_{wR}[1]$, and estimate $S_{oR}[2]$ from Eq. 8a. With this estimate fixed, make a new estimate of $S_{wR}[2]$ from Eq. 8b, and flip-flop until convergence. Usually a couple of iterations is sufficient.

Third General Reversal. The $p_{cd}[2]$ process is now scanning from $S_w[2]$ and back to $S_w[1]$. If a new reversal occurs at $S_w[3]$ before reaching $S_w[1]$, a $p_{ci}[3]$ process is set up, scanning from $S_w[3]$ and back again to $S_w[2]$. If the $p_{cd}[2]$ process should reach $S_w[1]$, however, and the water saturation continues to decrease, and the process reverts from a $p_{cd}[2]$ curve to a $p_{cd}[0]$ curve, i.e., it continues on the primary drainage curve.

More Reversals. The formalism can easily be generalized. Fig. 3 shows another example of a set of enclosing scanning loops between the bounding curves. Let us say that the history started with a primary drainage from $S_w = 1$ to S_{wR} ; then a first reversal, $S_w[1] = S_{wR}$, and the process traced the bounding imbibition curve until $S_w = 1 - S_{oR}$, where the second reversal occurred, $S_w[2] = 1 - S_{oR}$. Then the process followed the secondary drainage bounding curve until a third reversal at $S_w[3]$, the first reversal marked in Fig. 3. The process now scans back on the $p_{ci}[3]$ curve towards $S_w[2]$ but experiences a fourth reversal at $S_w[4]$. Then two more reversals occur, $S_w[5]$ and $S_w[6]$. After the sixth reversal, the process scans back on the $p_{cd}[6]$ curve to $S_w[5]$, passes through this point, and continues on the $p_{cd}[4]$ curve back

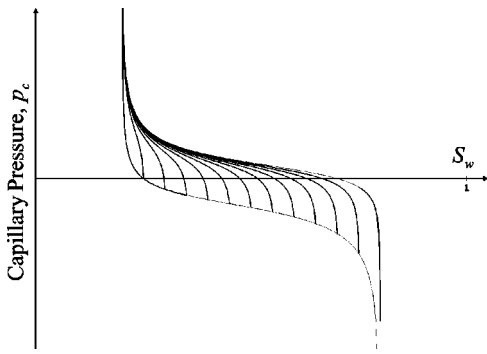


Fig. 4—Series of drainage scanning curves initiated at different reversal points on the imbibition bounding curve.

to $S_w[3]$ where it progresses on the $p_{cd}[2]$ curve, which, for this example, is the secondary drainage bounding curve.

Suite of Reversals From Bounding Curves. Several experimental papers^{16,19} report series of reversals from the imbibition and drainage bounding loops with features described above in design constraint No. 4. **Figs. 4 and 5** demonstrate that these features are well reproduced by the proposed hysteresis loop logic.

Bottom-Water Drive

The initial saturation distribution with height in a reservoir is usually determined by the primary drainage capillary pressure. When oil production starts, the free water level (FWL)—the elevation where $p_c=0$ —slowly moves upwards. The saturation at each height in the capillary transition zone between oil and water becomes a reversal saturation $S_w[1]$ for a scanning imbibition curve, each aiming at an $S_{oR}[1]$ value given by Eq. 4.

A sample calculation is shown in **Fig. 6**. The initial free water level, FWL_{in} , is at height 0 m and the corresponding saturation distribution is given by the primary drainage curve. Along this curve, a series of heights are selected for computational purposes. The saturation at each height will follow a unique scanning imbibition curve when the water level rises. When the FLW has reached 57 m, indicated by the dotted line in **Fig. 6**, the capillary pressure has decreased by the corresponding amount at each selected height. The saturation values are calculated from the individual imbibition scanning curves, rendering the new saturation distribution (dotted curve). This is an intermediate curve between primary drainage and the bounding imbibition curve. If the water level continues to rise, the intermediate curve will exhibit a permanent shape at high water saturations caused by residual oil saturations and will approach the bounding imbibition curve at low water saturations. This effect has been discussed by Kriebner and Heinemann.¹³

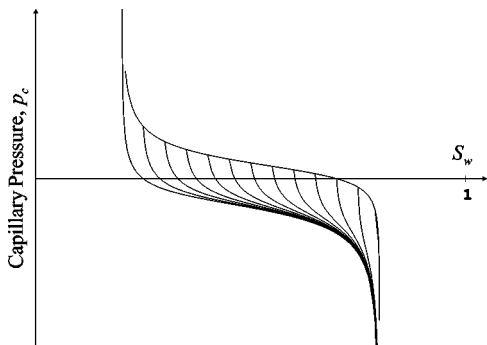


Fig. 5—Series of imbibition scanning curves initiated at different reversal points on the secondary drainage bounding curve.

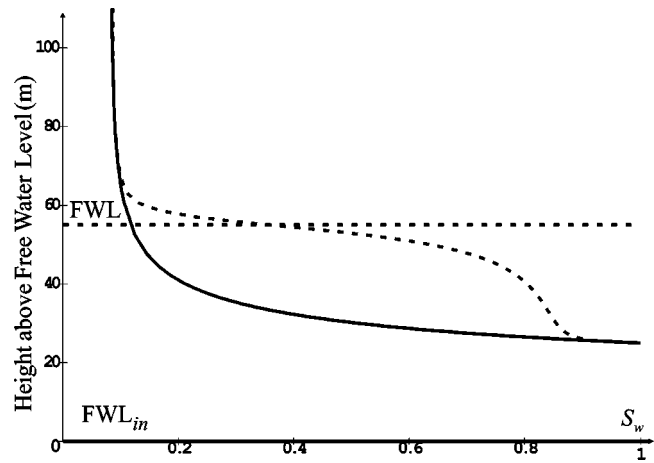


Fig. 6—Saturation distributions and associated FWLs for two values of the FWL: (1) the solid line and curve correspond to initial conditions. The FWL value is at zero height and the saturation distribution follows the primary drainage curve; (2) the dotted line shows the FWL at 57 m and the dotted curve shows the corresponding saturation distribution with an intermediate shape between primary drainage and imbibition bounding curves.

Validation

A capillary pressure correlation should have a minimum number of adjustable parameters yet be sufficiently flexible to fit a variety of measured datasets. Brooks and Corey^{2,3} have shown that this is case for the water branch of Eq. 2, and we will try to corroborate the full form of Eq. 2.

Centrifuge Bounding Curve Data. **Figs. 7 and 8** show the results of curve fitting the correlation to centrifuge data for two fresh core samples. The data are recorded from a forced imbibition and a forced secondary drainage process, i.e., half the water branch and half the oil branch are measured. This is a standard procedure by core laboratories. The curve fitting follows these steps.

1. When $S_w \rightarrow 1 - S_{oR}$, the oil branch dominates in Eq. 2, and a plot of $\log(-p_c)$ vs. $\log((S_o - S_{oR})/(1 - S_{oR}))$ according to

$$\log(-p_c) = \log(-c_{oi}) - a_{oi} \log\left(\frac{S_o - S_{oR}}{1 - S_{oR}}\right), \quad (9)$$

yields estimates of c_{oi} and a_{oi} . The lowest measured S_o value is used for S_{oR} .

2. With no data available from spontaneous secondary drainage, we assume that $a_{od} = a_{oi} = a_o$, the inverse pore size distribution index at low oil saturations.

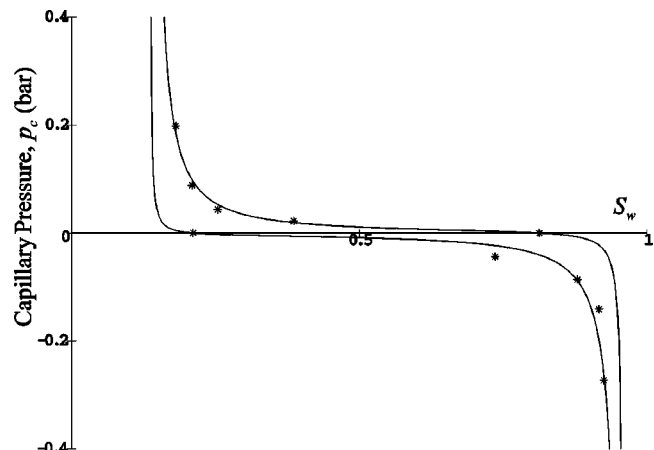


Fig. 7—Capillary pressure correlation fitted to forced imbibition and forced drainage centrifuge data from special core analysis.

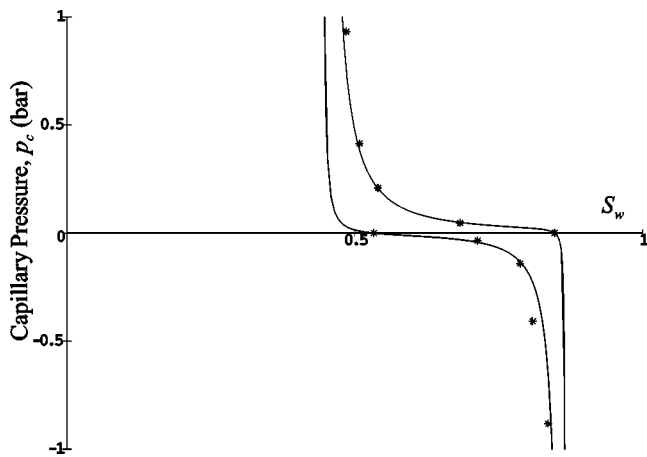


Fig. 8—Capillary pressure correlation fitted to forced imbibition and forced drainage centrifuge data for another core.

3. Since S_{w0i} is the known start saturation for forced imbibition, c_{wi} is found from Eq. 3a.

4. In the same manner estimates of c_{wd} and a_{wd} are determined from data points where $S_w \rightarrow S_{wR}$, and S_{wR} is set equal to the lowest measured water saturation; c_{od} is found from Eq. 3b.

5. It is assumed that $a_{wd} = a_{wi} = a_w$, the inverse pore size distribution index in the low water saturation range.

6. With these estimates of the parameters, an expression for the total error is made by summing the errors squared between a measured capillary pressure and the correlation value, Eq. 2. The errors are weighted by the factor $(1/p_c)^2$. The total error is simultaneously minimized with respect to a_o , a_w , c_{oi} , and c_{wd} by the optimization package, Microsoft Excel Solver, and c_{od} and c_{wi} are found by Eqs. 3.

The match in Figs. 7 and 8 is good, and this is also the case for all the other centrifuge results we have investigated.

Micropore Membrane Loop Data. We have matched a reported¹⁸ series of capillary pressure experiments on a fresh, oil-wet reservoir core to further check the applicability of the correlation and the hysteresis loop logic.

The core was not cleaned. It was saturated with dead crude oil and formation water and the last preparatory flow was a water-flood until no more oil was produced. Then the experiment followed this sequence (capillary pressures in mbar):

- drainage to +350 mbar,
- spontaneous imbibition, +350 → +1 mbar, bounding curve,
- forced imbibition, 0 → -350 mbar, bounding curve,

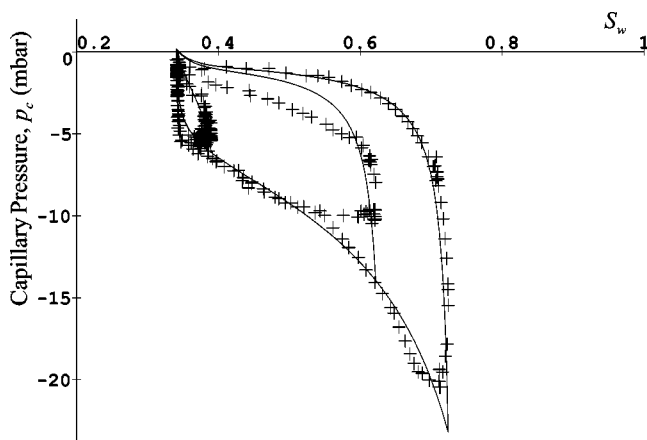


Fig. 9—Large, medium, and small scanning loop data and correlation curves shown together.

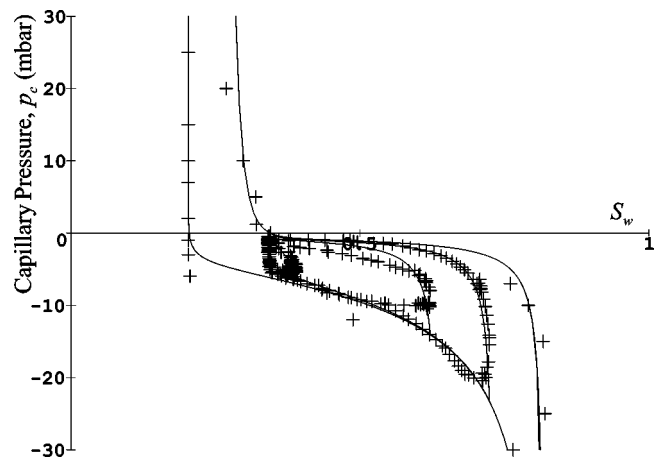


Fig. 10—All data and fitted curves shown together.

- spontaneous drainage, -350 → -1 mbar, bounding curve,
- scanning loop, -1 → -5 → -1 mbar, small,
- scanning loop, -1 → -10 → -1 mbar, medium,
- scanning loop, -1 → -20 → -1 mbar, large,
- forced drainage, 0 → +350 mbar, bounding curve.

In measurement series (a), an attempt was made to drive the system to S_{wR} to ensure that the rest of the steps are all within the bounding hysteresis loop.

First we fitted the bounding curves described above for the centrifuge data, assuming $a_{wi} = a_{wd}$ and $a_{oi} = a_{od}$. This gave a reasonably good overall match with only some discrepancy for measurement series (d). The fit improved when the a 's for drainage and imbibition were allowed to be different. Still, the match for the drainage part of the scanning loops could have been better. Since, on the assumption that the a 's and c 's are the same for all the curves, we decided instead to match the largest scanning loop and predict the medium and small scanning loops and the bounding curves.

The final match for the large scanning loop and the predicted medium and small scanning loops are shown together with the data points measured in Fig. 9. The scanning drainage curves for the medium and small loops are predicted by the hysteresis loop logic presented above. The only adaption is the choice of reversal points for the start of the drainage curves. In Fig. 10 also included are the predicted bounding curves together with the three scanning loops and all the data measured. Although further fine tuning could have been performed and the data contain some drift due to the ramping speed,¹⁸ the capillary pressure correlation and the hysteresis loop logic model the experiments satisfactorily.

Well Log Data From a Bottom-Water Driven Reservoir. In Fig. 11 is a plot of height above the free water level vs. water saturation for a well in a sandstone reservoir in the North Sea. The data were logged in 1989 before production started and follow a primary drainage curve, Eq. 1. Data from tight shale stringers were deleted from the match and no J -function normalization was attempted.

After production had started, the well was logged again in 1993 and 1994 with a carbon/oxygen tool. In 1994, the FWL had risen about 85 m and the data above the intermediate curve between primary drainage and imbibition may be fitted with a pure imbibition curve, as explained in the Bottom-Water Drive section. The signal-to-noise ratio is worse for the completed well and some of the data points have been removed. The result is shown in Fig. 12. The height of the FWL is now an additional matching parameter. From knowledge of the residual saturations S_{wR} and S_{oR} from the match, Land's trapping constant was determined by Eq. 4.

With all parameters fixed except the FWL, which was adjusted separately, the saturation distribution with height is predicted by the capillary pressure correlation for the 1993 data in Fig. 13, including the transition from primary drainage to imbibition modeled by scanning curves and the hysteresis logic. Some data points

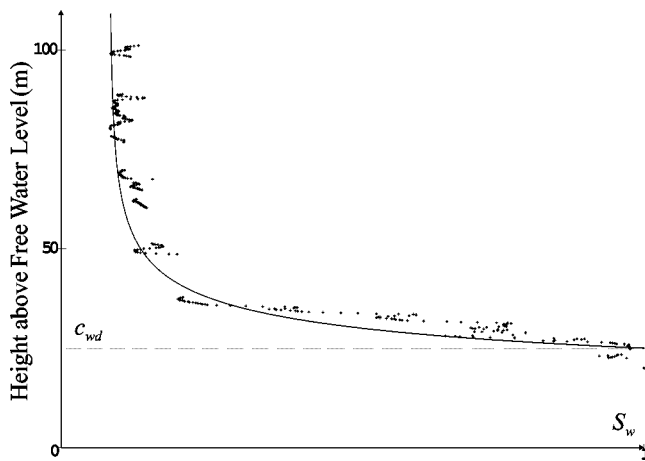


Fig. 11—Height above the free water level as a function of water saturation, well data, and fitted correlation, initial conditions, primary drainage.

were deleted and the rest were smoothed by a moving 10-point scheme. Although the match surely could have been improved, Fig. 13 demonstrates the ability of the correlation to forecast the water saturation distribution as the water table rises.

Relative Permeability Functions

The Corey-type⁶ or power-law expressions are popular correlations for relative permeability functions of water-wet reservoirs. They may be predicted from the primary drainage capillary pressure curve or fitted to measured relative permeability values. It seems reasonable that an extension to mixed-wet reservoirs would require symmetrization with respect to the two fluids, possibly along the following lines.

Let $k_{rw,wwd}$ denote the drainage relative permeability to water in a completely water-wet system, i.e., one derived solely from the water branch of the general capillary pressure correlation, Eq. 2, and let $k_{ro,wwd}$ denote the corresponding oil relative permeability. Then the Corey-Burdine^{6,21} expressions are

$$k_{rw,wwd} = S_{nw}^{3+2a_{wd}}, \quad k_{ro,wwd} = (1 - S_{nw}^{2a_{wd}+1})(1 - S_{nw})^2, \quad (10)$$

where

$$S_{nw} = \frac{S_w - S_{wR}}{1 - S_{wR} - S_{oR}} \quad (11)$$

for secondary drainage, with S_{oR} dropped for primary drainage.

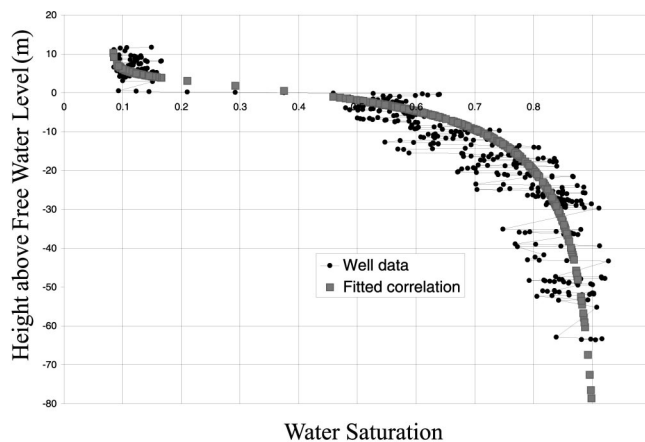


Fig. 12—Height above the free water level in 1994 as a function of water saturation, well data, and fitted correlation, imbibition bounding curve.

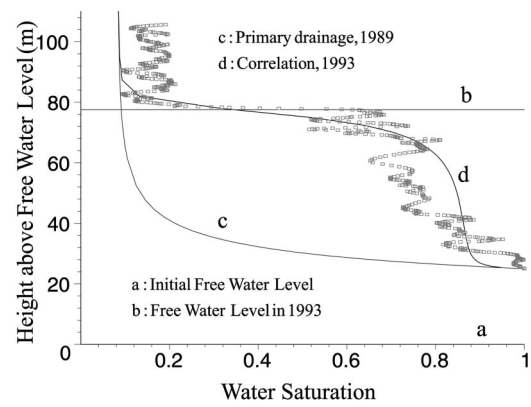


Fig. 13—Height above the initial free water level in 1993 as a function of water saturation, well data, and prediction by correlation, transition from primary drainage to imbibition bounding curve.

For a completely oil-wet system, solely from the oil branch of the capillary pressure correlation, we may write for the drainage oil and water relative permeabilities, respectively, as

$$k_{ro,owd} = S_{no}^{3+2a_{od}} \quad \text{and} \quad k_{rw,owd} = (1 - S_{no}^{2a_{od}+1})(1 - S_{no})^2, \quad (12)$$

where

$$S_{no} = \frac{S_o - S_{oR}}{1 - S_{wR} - S_{oR}}. \quad (13)$$

For a mixed-wet system, the water phase could be perceived to move partly as a wetting phase and partly as a nonwetting phase with relative strengths c_{wd} and c_{od} , the weight factors on the water and oil branches of the capillary pressure correlation, Eq. 2, implying the following expression for the drainage water relative permeability of the mixed-wet system,

$$k_{rwd} = \frac{c_{wd}k_{rw,wwd} - c_{od}k_{rw,owd}}{c_{wd} - c_{od}} \quad (14a)$$

and

$$k_{rod} = \frac{c_{wd}k_{ro,wwd} - c_{od}k_{ro,owd}}{c_{wd} - c_{od}} \quad (14b)$$

for the drainage oil relative permeability. Of course, Eqs. 14 represent just an educated guess of the shape of the correlations. Validation and possible modifications are needed based on con-

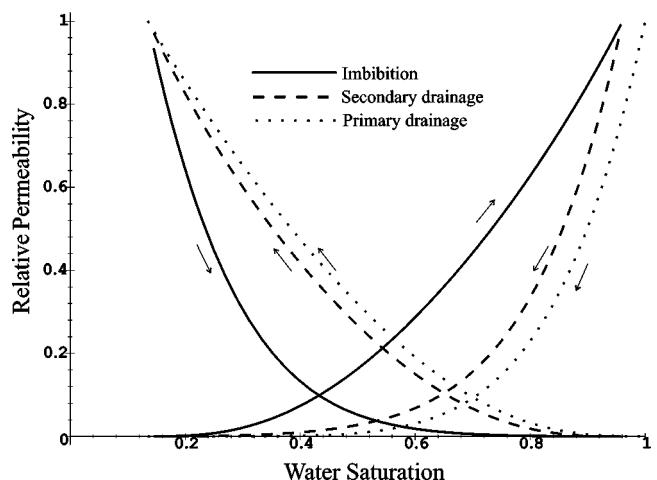


Fig. 14—Relative permeability curves for primary drainage, imbibition, and secondary drainage, data from Fig. 7.

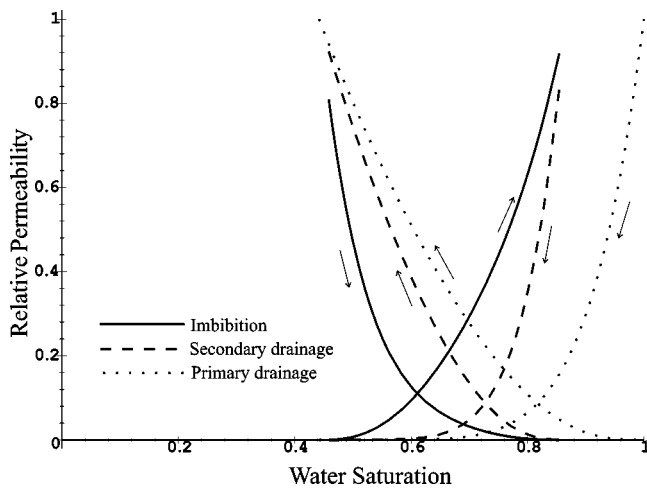


Fig. 15—Relative permeability curves for primary drainage, imbibition, and secondary drainage, data from Fig. 8.

sistent measurements of capillary pressure and relative permeability functions. For instance, endpoint relative permeability values at residual saturations for each of the Corey-Burdine expressions could be introduced as a modification.

As examples, **Figs. 14 and 15** show three pairs of relative permeability curves for oil and water: (1) primary drainage, (2) imbibition, and (3) secondary drainage. The a and c parameters of Eqs. 10, 12, and 14 are taken from the capillary pressure correlation fit of the centrifuge data in **Figs. 7 and 8**.

A relative permeability hysteresis loop logic should be designed to honor measurements^{22,23} and be consistent with the capillary pressure hysteresis loop logic.²⁴

Conclusions

1. A general capillary pressure correlation for mixed-wet rock was presented and its applicability demonstrated.
2. A new hysteresis scanning loop scheme was developed and validated by comparison with measurements.
3. The hysteresis scheme was employed to model the transition of the vertical saturation distribution in a reservoir from an initial primary drainage curve to an imbibition curve as the water table rises.
4. An extension of the Corey-type relative permeability correlation was suggested for mixed-wet rock.

Nomenclature

- a = constant, dimensionless
 c = constant, bar or mbar
 k_r = relative permeability, dimensionless
 p = pressure, bar or mbar
 C = Land's trapping constant, dimensionless
 I_w = wettability index
 S = saturation
 $[k]$ = scanning loop reversal k

Subscripts

- c = capillary
 d = drainage
 i = imbibition
 in = initial
 n = normalized
 o = oil
 ow = oil-wet
 R = residual
 r = relative
 w = water
 ww = water-wet
 AH = Amott-Harvey

0 = zero point ($p_c=0$)

Acknowledgment

We thank Den Norske Stats Oljeselskap A.S. (Statoil) for support and for permission to publish the article.

References

1. Bentsen, R.G. and Anli, J.: "Using Parameter Estimation Techniques to Convert Centrifuge Data into a Capillary-Pressure Curve," *SPEJ* (February 1977) **17**, 57; *Trans.*, AIME, **263**.
2. Brooks, R.H. and Corey, A.T.: "Hydraulic Properties of Porous Media," Hydraulic Paper No. 3, Colorado State U., 1964.
3. Brooks, R.H. and Corey, A.T.: "Properties of Porous Media Affecting Fluid Flow," *J. Irrigat. Drainage Div., Proc. ASCE* (1966) **92**, No. IR2, 61.
4. Parker, J.C. and Lenhard, R.J.: "A Model for Hysteretic Constitutive Relations Governing Multiphase Flow, 1. Saturation-Pressure Relations," *Water Resour. Res.* (1987) **23**, No. 12, 2187.
5. Huang, D.D., Honarpour, M.M., and Al-Hussainy, R.: "An Improved Model for Relative Permeability and Capillary Pressure Incorporating Wettability," paper presented at the 1997 Society of Core Analysts International Symposium, Calgary, 7–10 September.
6. Standing, M.B.: "Notes on Relative Permeability Relationships," *Proc.*, U. of Trondheim, NTH, Norway (1975).
7. Morrow, N.R.: "Wettability and Its Effects on Oil Recovery," *JPT* (December 1990) **42**, 1476; *Trans.*, AIME, **289**.
8. Jerauld, G.R. and Rathmell, J.J.: "Wettability and Relative Permeability of Prudhoe Bay: A Case Study in Mixed-Wet Reservoirs," *SPEJ* (February 1997) **12**, 58.
9. Leverett, M.C.: "Capillary Behaviour in Porous Solids," *Trans.*, AIME (1941) **142**, 152.
10. Hamon, G. and Pellerin, F.M.: "Evidencing Capillary Pressure and Relative Permeability Trends for Reservoir Simulation," paper SPE 38898 presented at the 1997 SPE Annual Technical Conference and Exhibition, San Antonio, Texas, 5–8 October.
11. Killough, J.E.: "Reservoir Simulation with History-Dependent Saturation Functions," *SPEJ* (February 1976) **16**, 37; *Trans.*, AIME, **261**.
12. Tan, T.: "Representation of Hysteresis in Capillary Pressure for Reservoir Simulation Models," *J. Cdn. Pet. Tech.* (July–August 1990) **29**, No. 4, 84.
13. Kriebenberg, M. and Heinemann, Z.: "A New Model for History Dependent Saturation Functions in Reservoir Simulation," paper presented at the 1996 European Conference on the Mathematics of Oil Recovery, Leoben, Austria, 3–6 September.
14. Kleppe, J. et al.: "Representation of Capillary Pressure Hysteresis in Reservoir Simulation," paper SPE 38899 presented at the 1997 SPE Annual Technical Conference and Exhibition, San Antonio, Texas, 5–8 October.
15. Land, C.S.: "Calculation of Imbibition Relative Permeability for Two- and Three-Phase Flow from Rock Properties," *SPEJ* (June 1968) **8**, 149; *Trans.*, AIME, **243**.
16. Morrow, R. and Harris, C.C.: "Capillary Equilibrium in Porous Materials," *SPEJ* (March 1965) **5**, 15; *Trans.*, AIME, **234**.
17. Wardlaw, N.C. and Taylor, R.P.: "Mercury Capillary Pressure Curves and the Interpretation of Pore Structure and Capillary Behaviour in Reservoir Rocks," *Bull. Can. Pet. Geol.* (June 1976) **24**, No. 2, 225.
18. Hammervold, W.L. et al.: "Capillary Pressure Scanning Curves by the Micropore Membrane Technique," *J. Pet. Sci. Eng.* (1998) **20**, 253.
19. Topp, G.C. and Miller, E.E.: "Hysteretic Moisture Characteristics and Hydraulic Conductivities for Glass-Bead Media," *Soil Sci. Soc. Am. Proc.* (1966) **30**, 156.
20. Colonna, J., Brissaud, F., and Millet, J.L.: "Evolution of Capillarity and Relative Permeability Hysteresis," *SPEJ* (February 1972) **12**, 28; *Trans.*, AIME, **253**.
21. Burdine, N.T.: "Relative Permeability Calculations from Pore Size Distribution Data," *Trans.*, AIME (1953) **198**, 71.
22. Braun, E.M. and Holland, R.F.: "Relative Permeability Hysteresis: Laboratory Measurements and a Conceptual Model," *SPEJ* (August 1995) **10**, 222.
23. Honarpour, M.M., Huang, D.D., and Al-Hussainy, R.: "Simultaneous Measurements of Relative Permeability, Capillary Pressure, and Electrical Resistivity with Microwave System for Saturation Monitoring," *SPEJ* (September 1996) **1**, 283.
24. Kjosavik, A.: "Integrated Modeling of Relative Permeability and Capillary Pressure," MS thesis, Stavanger College, Stavanger, Norway (1999).

SI Metric Conversion Factorsbar \times 1.0*

E+05=Pa

*Conversion factor is exact.

SPEREE

Svein M. Skjaeveland is a professor of petroleum engineering at Stavanger College. e-mail: s-skj@hsr.no. He holds a PhD degree in physics from the Norwegian U. of Science and Technology and a PhD in petroleum engineering from Texas A&M U. Skjaeveland is a member of the Editorial Review Committee for *SPE Reservoir Evaluation & Engineering*. **Leiv Magne Siquveland** is a well log engineer with Maritime Well Service in Norway. e-mail: lmsiqveland@hotmail.com. He holds a BS degree in telecommunication and an MS degree petroleum engineering, both from Stavanger College. **Arnfinn Kjosavik** is a reservoir engineer with Statoil. e-mail: arkjo@statoil.com. He

holds BS and MS degrees in petroleum engineering from Stavanger College. **Wibeke Hammervold Thomas** is a senior engineer with Statoil, working on reservoir evaluation. e-mail: wiha@statoil.com. Previously, she was a research scientist with RF-Rogaland Research. She holds BS and MS degrees from Stavanger College and a PhD degree from Aalborg U. in Denmark, all in petroleum engineering. **George A. Virnovsky** is chief scientist in the Reservoir Technology/Geolog Group at RF-Rogaland Research in Stavanger. e-mail: George.Virnovsky@rf.no. Previously, he worked as a senior research scientist at the All-Russian Scientific Research Inst. (VNII) in Moscow. Virnovsky holds an MS degree in electrical engineering from Gubkin Academy in Moscow and a PhD degree in reservoir engineering from VNII. His research interests include reservoir simulation, fluid flow in porous media, and core analysis.